Mechanics of F-Actin Characterized with Microfabricated Cantilevers

Xiumei Liu and Gerald H. Pollack
Department of Bioengineering, University of Washington, Seattle, Washington 98195 USA

ABSTRACT In this report we characterized the longitudinal elasticity of single actin filaments manipulated by novel silicon-nitride microfabricated levers. Single actin filaments were stretched from zero tension to maximal physiological tension, P_0. The obtained length-tension relation was nonlinear in the low-tension range (0–50 pN) with a resultant strain of ~0.4–0.6% and then became linear at moderate to high tensions (~50–230 pN). In this region, the stretching stiffness of a single rhodamine-phalloidin-labeled, 1-μm-long F-actin is 34.5 ± 3.5 pN/nm. Such a length-tension relation could be characterized by an entropic-enthalpic worm-like chain model, which ascribes most of the energy consumed in the nonlinear portion to overcoming thermal undulations arising from the filament's interaction with surrounding solution and the linear portion to the intrinsic stretching elasticity. By fitting the experimental data with such a worm-like chain model, an estimation of persistence length of ~8.75 μm was derived. These results suggest that F-actin is more compliant than previously thought and that thin filament compliance may account for a substantial fraction of the sarcomere's elasticity.

INTRODUCTION

F-actin is a critical component of myofibril and of virtually all eukaryotic cells, yet its elastic behavior remains unclear. Early studies of muscle (Huxley and Simmons, 1971; Ford et al., 1977, 1981) attributed almost all of the sarcomere's elasticity to cross-bridges rather than to filaments. However, recent investigations on F-actin elasticity either by x-ray diffraction (Huxley et al., 1994; Wakabayashi et al., 1994; Bordas et al., 1999) or light-scattering methods (Higuchi et al., 1995) showed that during the rise of isometric tension, the length of thin filaments increased by 0.2–0.42%. Other studies of actin-filament flexibility, either by laser traps (Dupuis et al., 1997; Adami et al., 1999) or by observations of thermal undulations (Oosawa, 1977, 1980; Oosawa et al., 1977; Yanagida et al., 1984; Gittes et al., 1993; Kas et al., 1984, 1996; Ott et al., 1993) revealed significant thin filament extensibility as well.

Nevertheless, the only substantive stiffness measurements made directly on single F-actin were carried out by Kojima and colleagues (1994). However, their measurement method provided only the stiffness at a specific high-tension point rather than along the entire force-extension curve. Due to the constraint of low trapping stiffness, F-actin stiffness measurements made by the use of optical tweezers were subjected to low tensions compared with the maximal physiological value (Dupuis et al., 1997; Adami et al., 1999). So far as we know, no complete description of the force-extension relation of single filament extension has appeared.

In this study we used novel microfabricated cantilevers to manipulate single actin filaments and obtained complete length-tension curves from zero to maximum physiological tension, P_0.

Submitted August 28, 2001, and accepted for publication June 13, 2002.

Address reprint requests to Dr. Gerald H. Pollack, University of Washington, Department of Bioengineering, 313 Harris Hydraulics Lab, WD-12, Box 357962, Seattle, WA 98195. Tel.: 206-685-1880; Fax: 206-685-3300; E-mail: ghp@u.washington.edu.

0006-3495/02/11/2705/11 $2.00

MATERIALS AND METHODS

Sample preparations

Actin filaments, polymerized from G-actin at the concentration of 0.8 mM (33.3 μg/ml) were prepared as described by Pardee and Spudich (1982) and provided courtesy of A. M. Gordon and C. Luo (Department of Physiology and Biophysics, University of Washington, Seattle, WA). Filaments were rhodamine-phalloidin (Molecular Probes, Eugene, OR) labeled and diluted in actin buffer AB (25 mM imidazole-HCl, pH 7.4, 25 mM KCl, 4 mM $MgCl_2$, 1 mM EGTA, and 1 mM dithiothreitol) to 4 nM just before use.

α-Actinin (Sigma Chemical Co., St. Louis, MO) purified from chicken gizzard was dialyzed against AB. It was used to coat the nitrocellulose-treated levers and increase their affinity to F-actin. Optimal coating concentration of α-actinin was ~4 mg/ml. Concentrations were checked by using a Biorad assay.

Cantilevers and flow cell

Microfabricated cantilever transducers made of thin silicon nitride (SiN_3) film (Fauver et al., 1998) were used to manipulate filaments (Fig. 1, *a* and *b*). Levers were fabricated in pairs to allow for differential measurements. One beam was used as a static reference and the other as transducer. One advantage of levers over other molecule-manipulation methods such as optical traps and glass needles is that all cantilevers fabricated in one batch show high stiffness consistency (±~7–16%) owing to the high precision of the microfabrication technique. Hence, stiffness calibrations of representative samples are sufficient to characterize the entire batch with satisfying accuracy. In addition, the wide tension range of cantilevers allowed us to exert tensions as large or small as required.

In earlier experiments on thick filaments, one of the two thickest of the lever set was used as a stationary reference beam (Neumann et al., 1998). For single actin filaments, however, we found that an unacceptably large fraction of the filaments' length would often stick to the reference beam, leaving only a short free segment available for manipulation. Therefore, in current experiments, flexible levers of the same stiffness were used at both ends. To get high accuracy of force measurement (corresponding to large displacement for the same required tension), the most flexible levers were adopted, whose stiffness, calibrated by monitoring the lever's resonant frequency (Fauver et al., 1998), was ~180 pN/nm.

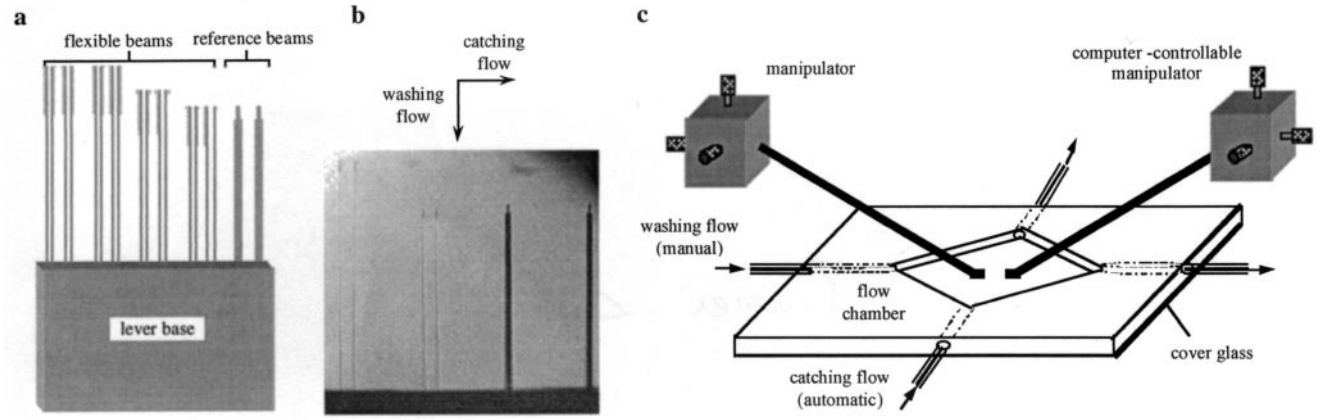

FIGURE 1 Nanofabricated levers (*a* and *b*) and flow cell (*c*). (*a*) Schematic structure of lever sets. The frame contains four pairs of flexible levers, all of which have the same dimensions except shaft length. The left-most two pairs are the most flexible with stiffness of 179 pN/nm and length of 568 μm. The other two flexible lever pairs have higher stiffness because of their shorter lengths. The right-most two levers were used as reference beams for experiments with thick filaments because of their high stiffness in comparison with filaments (Neuman et al., 1998). The other ends of levers are fixed to the silicon base, which is solidly stuck to a metal rod held by a piezoelectrically driven manipulator. (*b*) Optical micrograph of lever beams. (*c*) Flow cell and arrangement of levers. Two lever pairs in the center of the flow cell are positioned by two manipulators. One lever pair is controllable by a Macintosh computer to automatically stretch and release captured filament. Arrows indicate the direction of solution flow.

The flow cell (see Fig. 1 *c*) was constructed from a plastic chamber and a cover glass (22 mm × 40 mm), sealed by Dow Corning grease. Four small holes were incorporated to facilitate pumping the solutions in and out of the cell, either manually or automatically. The manual hole-pair could guide solution parallel to the levers and was used to wash excess α-actinin away after the levers had been incubated in α-actinin. The other hole-pair, controlled by two automatic syringe pumps (Yale Apparatus, Multi-phaser, model YA-12) was used for flowing filaments perpendicularly to lever beams to aid the F-actin capture.

Experimental procedures

After being fixed in the flow cell (see Fig. 1 *c*), the two lever pairs were incubated in 10 μl of α-actinin at 4 mg/ml for ~5–10 min, followed by the washing of excess proteins out of the cell with AB. Then the chamber was pumped almost dry so that filament suspensions (4 nM) could be added as close as possible to the lever pairs. This approach minimized the required amount of F-actin. Immediately after the addition of F-actin, an oxygen scavenger system (3 mg/ml glucose, 0.018 mg/ml catalase, 0.1 mg/ml glucose oxidase, and 20 mM dithiothreitol in AB/bovine serum albumin) was pumped into the cell at a speed of 0.5 ml/min to attenuate photo bleaching. The flow guided filaments perpendicularly to the lever shaft so that they could be captured more efficiently than freely floating ones. As a result, free filaments were also washed out of the field of view.

Optical system

The Zeiss Axiovert 135 TV microscope system used for these experiments is shown schematically in Fig. 2. The flow chamber was placed on the translation stage. The cover glass of the flow cell was coupled to a ×100 oil-immersion objective (Zeiss Plan-Neofluar, ×100/1.30 oil), and the chamber solution was coupled to a water-immersion condenser (Zeiss Achroplan, ×63/0.9 W). The two lever pairs were both controllable by piezoelectrically driven manipulators (model Ts-5000–150, Burleigh, New York, NY), one of which could also be automatically driven by a Macintosh computer.

This apparatus could work in two alternative modes by simply switching the position of slider 1: bright-field for lever movements measurement

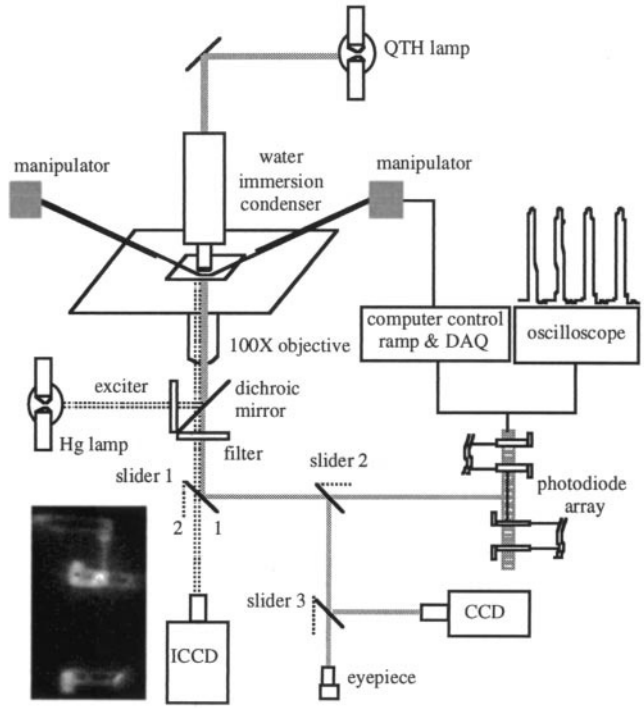

FIGURE 2 Optical system for experiments: bright-field (slider 1 at position 1) and fluorescence (slider 1 at position 2) microscope. The thick gray solid lines show the optical path of bright-field observations (CCD) and measurements of lever movement (photodiode array). The double dashed lines show the optical path of the fluorescence microscope. The computer was used to generate ramp waveform and for data acquisition (DAQ). The schematic oscilloscope waveform shows lever peaks from the photodiode array. The picture shown at bottom left is the fluorescence image of a captured actin filament between two levers.

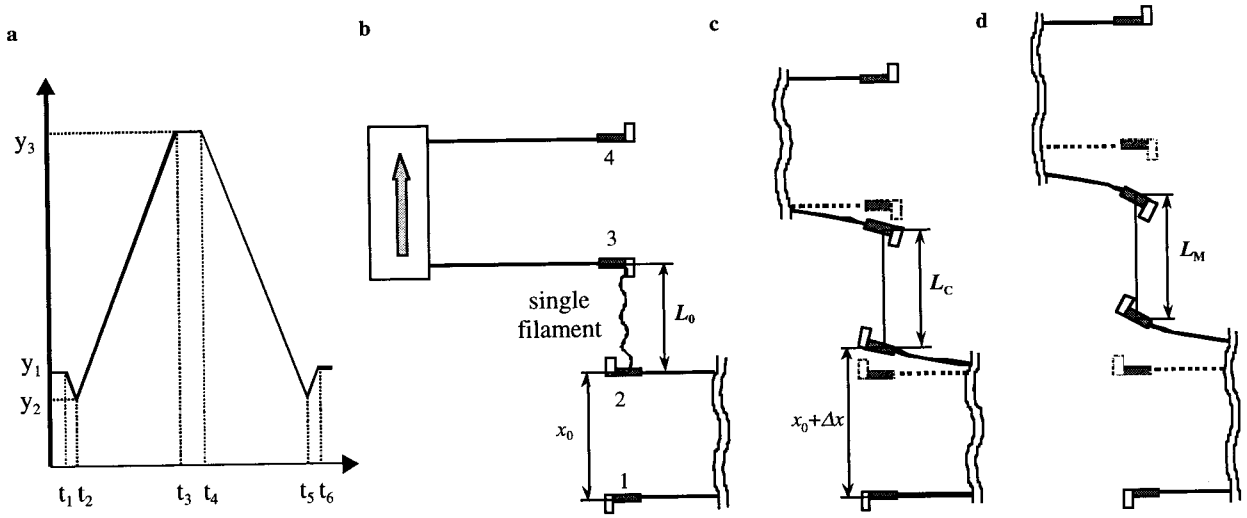

FIGURE 3 Ramp waveform (*a*) and measurement method (*b–d*). (*a*) The waveform was used to stretch and release the captured filaments. The y_1, y_2, and y_3 are displacements of moveable levers. See text for details. (*b—d*) Schematic diagram of the relationship between lever movement and filament elongation. L_0 is the initial length, and L_c is the contour length, as defined in the text describing the WLC model. L_m is the maximal length that the filament reached. x_0 is the initial separation between the two levers before the filament was stretched, and Δx is the deflection of lever beam.

and fluorescence for the visualization of levers and F-actin. For bright-field mode, the flow cell was illuminated by an intensity-adjustable quartz-tungsten-halogen light source. The magnified images of lever pairs were projected onto an 1024-pixel photodiode array (RL1024K, EG&G, Reticon, Sunnyvale, CA). Before attempting to catch a filament, the lever pairs' positions and light intensity were optimized for the sake of stable lever peak shape and signal level. The apparatus was then switched to fluorescence mode, whose light source was a 100-W mercury arc lamp (HBO 100, Zeiss Attoarc, Thornwood, NY) directed through an optical fiber coupling (Technical Video, Woods Hole, MA). Fluorescence images of levers and filaments (see bottom left of Fig. 2) were monitored by a silicon-intensified camera (Sony XC-77 CCD, Sony Electronics, San Jose, CA).

Once a single actin filament was caught at both ends, the apparatus was switched again to the bright-field mode. Consequently, the levers' positions were collected by a computer continuously at a pixel sampling rate of 50 kHz. The magnification is 10 pixels/μm, implying that the position of a lever would change 10 pixels on photodiode array if the movement is 1 μm. The peak width of flexible beams is ~40 pixels. To achieve sub-pixel resolution, the peak centroid were analyzed by software. In addition, to prevent the filament from detaching or breaking because of the mechanical disturbance caused either by inserting slider 1 or pulling out the filter set (exciter/dichroic mirror/emitter: 642 nm/595 nm/629 nm; Chroma Technology Corp., Brattleboro, VT), the notch position of slider 1 was changed so that slider 1 could be switched smoothly and the filter set was kept in the optical path during bright-field measurements. The entire apparatus rested on an active vibration-isolation system (Integrated Dynamics Engineering, Westwood, MA).

Measurement method

The measurements began with one of the two manipulators driven automatically, following a computer-generated ramp waveform to stretch and then release the filament (Fig. 3 *b*, *arrow*). Generally, we used the waveform shown in Fig. 3 *a*. That is, when a filament was caught, sometimes it had already been slightly stretched beyond its slack length ($F > 0$). To obtain a complete stretch-release curve starting from zero tension ($F = 0$), the filament was released slightly ($t_1 \rightarrow t_2$) before stretching ($t_2 \rightarrow t_3$). When tension reached the desired maximal value ($F \approx 230$ pN), as determined from the movable levers' displacement, lever position was held constant for 1 s ($t_3 \rightarrow t_4$) before release ($t_4 \rightarrow t_5$).

The stretching process is shown schematically in Fig. 3, *b–d*. At first, the nonmovable lever pair 1–2 had a separation of x_0, and the filament had an initial length of L_0. With the increase of the displacement of the movable lever pair (indicated by an *arrow*), F-actin was continuously stretched, and the separation of lever pair 1–2 increased by Δx. During the stretch/release cycle, lever positions were tracked continuously by the photodiode array. By subtracting the positions of lever 3 from 2, the variation of filament length L at different tension levels could be obtained. Similarly, the deflection Δx of lever 2 could be obtained by subtracting the position of lever 2 from 1. Then, the tension could be deduced by the application of Hooke's law:

$$F = k_l \Delta x, \tag{1}$$

where k_l is the lever stiffness and F is the exerted tension. It should be pointed out that the captured filament was sometimes not at the lever tip but tens of microns away, along the lever shaft. In such cases the real lever stiffness k_l was recalculated by the following expression (Fauver et al., 1998):

$$k_l \propto \frac{E}{l^3}, \tag{2}$$

where E is Young's modulus, a constant determined by material characteristics, and l is the length of the cantilever measured from its base to the actual attachment point of filament.

RESULTS

Typical length-tension curve

A typical length-versus-tension curve of a single F-actin filament is shown in Fig. 4 *a* with the stretch portion demonstrated by open circles and the release portion by plus marks. In terms of slope (stiffness), the curves could be

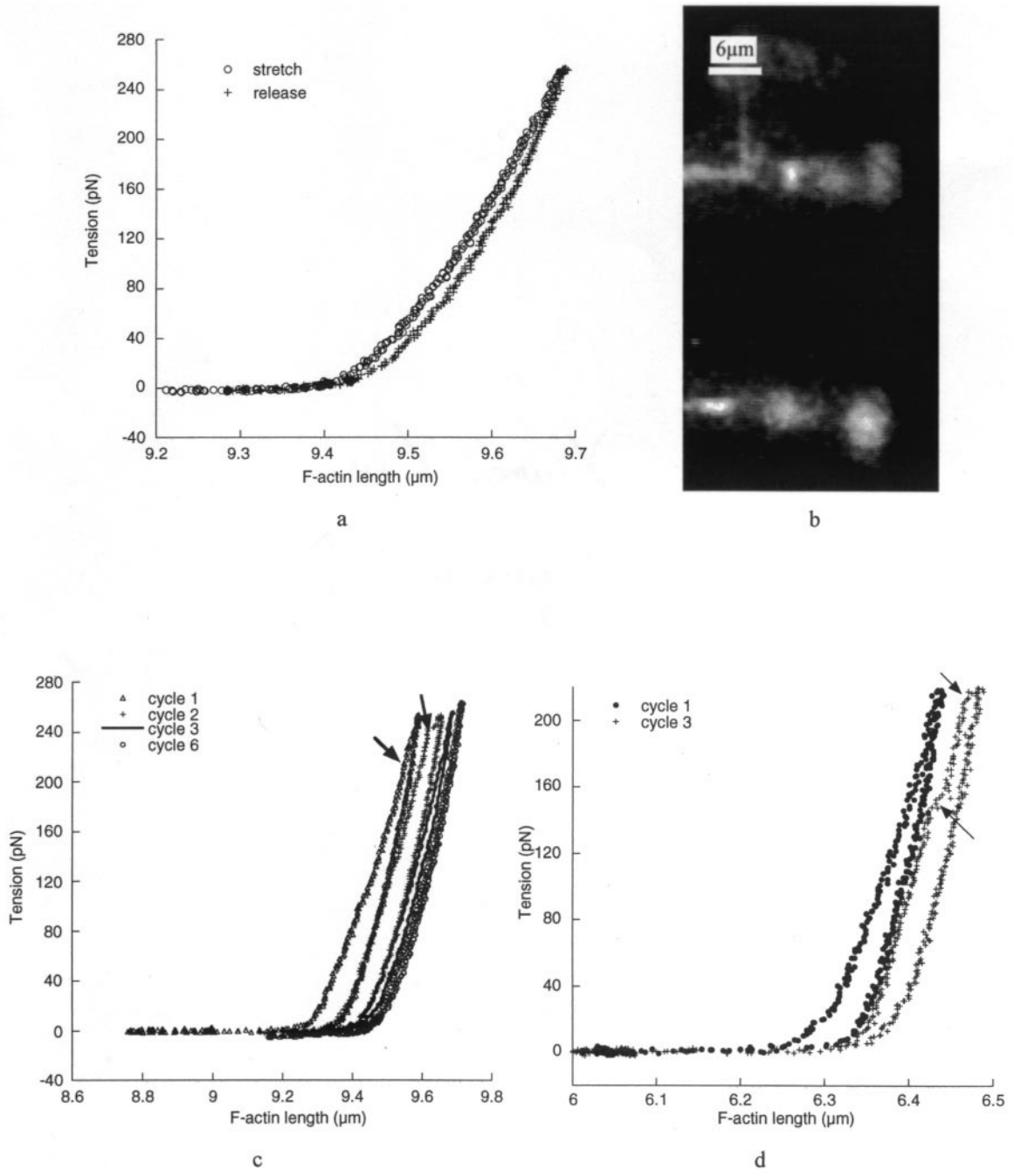

FIGURE 4 (*a*) Relationship between length and tension of a single filament. The total time duration for one stretch-release cycle is 12 s, and that of stretch ($t_2 \rightarrow t_3$ in Fig. 3 *a*) and release segments ($t_4 \rightarrow t_5$ in Fig. 3 *a*) are each 4 s. Maximum tension in this record is ~12% higher than maximal physiological value (230 pN). (*b*) Fluorescence image of the captured actin filament and levers. (*c*) Six cycles for the same filament as that of *a*. For clarity, only four of six cycles are shown. (*d*) As the filament was stretched within the physiological tension range, sudden changes of slope appeared sometimes, as indicated by arrows.

divided into two portions. In other words, when tension is low, the curves are nonlinear, implying a nonconstant stiffness, whereas at moderate and high tensions, they are almost linear.

Generally, several stretch-release cycles could be accomplished before filaments broke. Four of six successive cycles from the same filament as Fig. 4 *a* are shown in Fig. 4 *c*. These curve cycles show reasonable stiffness reproducibility. However, the curves did not return to the same initial length, which is especially obvious in the first cycle. Such behavior is responsible for the sequential rightward shift of the curves and the hysteresis.

The most obvious differences among these curves resided in the stretch portions. The slopes sometimes became abruptly lower, frequently at high tensions, as indicated by the arrows in the first two cycles of Fig. 4 *c*. This happened before the stop of the movable lever pair ($t_3 \rightarrow t_4$ in Fig. 3 *a*).

Such behavior was also found when tension was well below the maximal physiological tension P_0, as indicated by arrows in Fig. 4 *d*. Therefore, overstretch beyond P_0 could be excluded as a basis. Another conspicuous feature of such abrupt slope changes is that they hardly occurred during the release phase. Hence, they promoted an increase of hysteresis. For example, the first two cycles of Fig. 4 *c* have more hysteresis than the others.

The origin of such sudden changes might lie in the sudden phase transition of segmental actin filament because of strain. As pointed out by Schutt and Lindberg (1992), for example, double-stranded F-actin can untwist from an α-helix into a ribbon, which is ~20% longer than that of α-helix. However, in our condition, only the actin filament itself was investigated, which means no myosin-actin interactions were available to induce such a conformational change. Therefore, such a phase transition might not be the explanation of the sudden F-actin elongation. A likely cause may be the nonrigid connections between filaments and levers, either because of the filaments' sliding along lever surface or because of sudden rupture/elongation of α-actinin–F-actin (see below).

Another significant feature of these curves is that at maximal tension, when the stretching movement stopped for 1 s before release, filament extension ceased accordingly, suggesting that actin filaments do not show viscoelastic behavior, at least at the investigated temporal scale. Thus, the stretching rate has no influence on curve slopes.

We also carried out some experiments without purposefully releasing filaments before initiating each stretch-release cycle. In such instances, most of the curves showed only the linear portion (Fig. 5). Only in the first cycle of Fig. 5 was the filament stretched from zero tension. At high tension, the elongation increased abruptly with negligible change of tension. This phenomenon is especially conspicuous in cycle 3, where, at maximal tension, there was a sudden length increase of ~50 nm. Upon release, the filament did not return to its initial length; also, the tension at the stop point was no longer zero (zero tension indicated by the *arrow*). In successive cycles, the same phenomenon was found, albeit smaller in magnitude. The failure of filament length to return to its initial value in each cycle is similar to that of Fig. 4 and may also be for the same reason, i.e., the rupture of connection.

Of 42 filaments studied, all experiments showed similar length-versus-tension relationships, in either Fig. 4 or Fig. 5, depending on the type of ramp input (with or without prerelease). The only significant difference among curves was the variation of slope at the linear portion, which resulted from filaments of different lengths. As shown in Fig. 6, a filament 3.3 μm long demonstrated a strain of almost 10% in the overall tension range whereas the shorter filament shown in Fig. 4 showed a strain of only ~3% at the same tension. These discrepancies seemed potentially explainable by the contribution of the F-actin connection to the lever. The connection compliance contributes relatively more when the filament is short than when it is long. Therefore, the question arose as to how the connection influences the curve shape and slope.

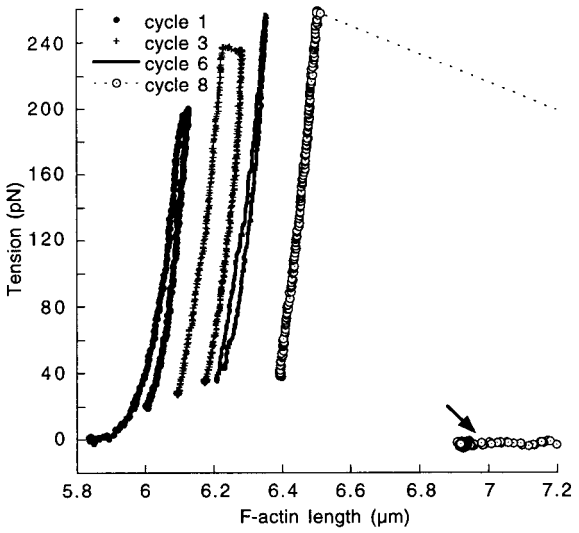

FIGURE 5 Length-versus-tension curves obtained without prereleasing the filaments in each cycle. For clarity, only four of eight cycles are shown. In the 8th cycle the filament broke and tension dropped back to zero, as indicated by an arrow.

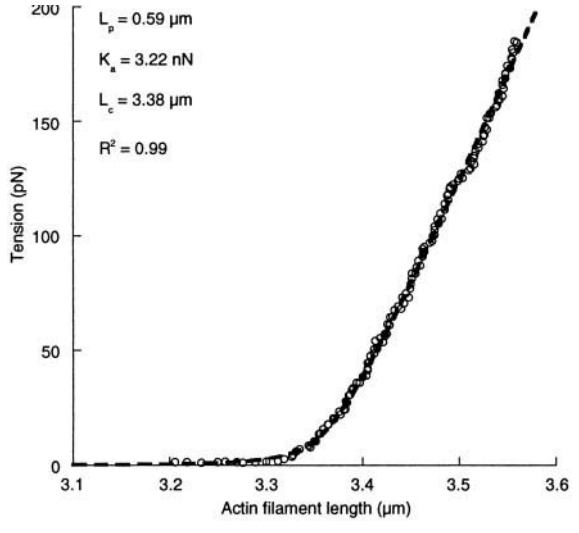

FIGURE 6 Relationship between length and tension of a single filament whose length is as short as 3.3 μm. In most of the tension range, the curve is almost linear.

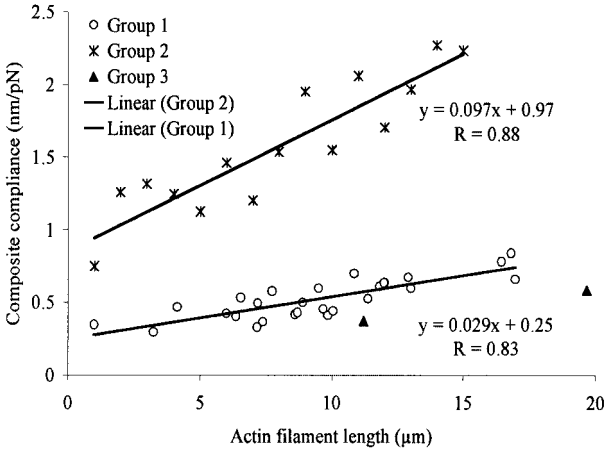

FIGURE 7 Relationship between filament length l and the composite compliance $1/K_{com}$. The data could be divided into three groups, each of which is indicated by different symbols. The equations show the linear fits to those data sets.

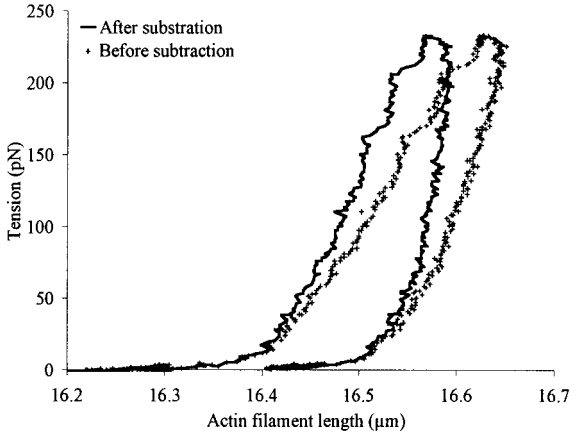

FIGURE 8 The influence of connection compliance on curve shape and stiffness: +, the original experimental data; ——, the same data after the exclusion of connection compliance.

Influence of the actin-lever connection

We evaluated the connection influence based on the results obtained from many filaments and then subtracted its contribution.

Consider the linear portion of length-tension curve. According to the description above, the measured extension is linearly related to the imposed tension. Therefore, a constant stiffness is expected.

However, such an obtained stiffness is a composite of connection stiffness and F-actin stiffness. In other words, the measured total compliance, or the reciprocal of stiffness, $1/K_{tot}$, should be the sum of the connection compliance $1/K_{con}$ and F-actin compliance l/K_a:

$$\frac{1}{K_{tot}} = \frac{l}{K_a} + \frac{1}{K_{con}} \tag{3}$$

In theory, the connection stiffness should have a consistent compliance independent of each experiment so that we can expect a linear relation between different filament lengths, l (widely variable from experiment to experiment) and $1/K_{tot}$ with a slope of $1/K_a$ and y-intercept $1/K_{con}$.

The relationship is shown in Fig. 7, derived from 42 filaments (140 stretch-release cycles). During the data analysis we found that if the filament had been stretched by more than one cycle, the hysteresis of the second and subsequent curves was much smaller than that of the first cycle. In this case, the stiffness of different cycles was averaged, whereas for those curves showing apparently smaller slopes, the stiffness was excluded from analysis, because we believe that hysteresis might be caused by an unstable connection during the first stretch.

As shown in Fig. 7, the data could be divided into three groups. Group 1 (26 filaments, lower plot) accounted for ~62% of the data. From its linear fit, the stiffness of a 1-μm-long filament during stretch and the stiffness of the connection are deduced to be 34.5 ± 3.5 pN/nm and 4.0 ± 0.42 pN/nm, respectively. For release, the F-actin stiffness was ~15–20% higher, namely, ~40–44 pN/nm.

These two values imply that when F-actin is as long as 10 μm, the extension of F-actin will contribute only ~50% to the measured elongation. The shorter the filament, the more influential was the connection on curve shape. It was also found that when F-actin is shorter, tension at the start point of the linear portion was lower. It implies that the amplitude of the nonlinear portion depends on filament length and that the connection has a linear elongation-tension relation. Thus, it is reasonable to assume that the connection mainly shows influence on the slope of the linear portion.

If we take ~40 pN/nm for micron-long filaments as real stiffness, the elongation of connection can be calculated by dividing tension by the connection stiffness. Hence, by simple subtraction, the relationship between the real actin elongation and tension can be obtained. Fig. 8 shows the curves before and after subtraction of a constant connection stiffness of 4.0 pN/nm. The curve shape hardly changes. Only the linear portion is shifted leftward, implying a stiffness increase.

Group 2 accounts for ~35% of the data (12 filaments, Fig. 7, upper plot). One feature in common for these data is that along almost the entire tension range the length-tension curves are linear. The start point of the linear portion is as low as ~5 pN and sometimes even zero tension. A representative data set was shown in Fig. 6. For filaments of group 1, on the other hand, this value could be as high as ~50 pN when filaments were long (see Fig. 9). By using the same method of linear fit as group 1, the deduced connection stiffness is as small as ~1.1 pN/nm, and filament stiffness of 1-μm-long filaments was 5.8 pN/nm. Both are

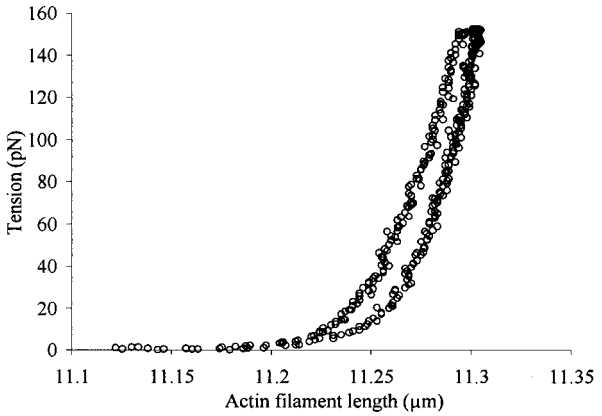

FIGURE 9 Relationship between extension and tension of a single filament when connection compliance had little influence on curve shape.

much smaller than those of group 1. The existence of this data group has two potential explanations.

From the smaller value of connection stiffness relative to that of group 1, one possibility is that there might be another kind of connection, which is more compliant. For example, suppose one end of the filament was held by the type of connection of group 1, whereas the other end slid continuously along the lever surface. Such slippage would be taken as a highly compliant connection and would make a large contribution to the measured elongation. In this case, the extension should be irreversible upon release. However, it was often found in filaments of group 2 that the traces of stretch and release were almost superimposable. Furthermore, an anomalous connection cannot explain the small actin-filament stiffness. For the same reason, the related possibility that filaments might be caught by some flexible lever-surface contaminant rather than α-actinin is also not valid.

A second possible explanation is that F-actin may have two states. Schutt and Lindberg (1992) proposed that F-actin can exist either in a helical configuration or ribbon-like configuration, with the subunit repeat of the latter ~20% larger than the former. The second group could reflect filaments that had been converted into the high-compliance, ribbon-like state. The F-actin of this ribbon-like state might have a different mode of connection with α-actinin relative to group 1.

The two data points marked as group 3 in Fig. 7 showed stiffness of 1-μm-long actin filaments as high as 33.3 pN/nm and 30.0 pN/nm, respectively. Apparently, they could not be incorporated into group 2 because of their high stiffness. We also attempted to include them in group 1. Doing so resulted in a much poorer linear regression (R = ~0.4) and very high F-actin stiffness, ~50 pN/nm. Hence, we did not include them in either group. Their stiffness is in good accordance with the statistical stiffness of group 1, 34.5 pN/nm. Hence, a reasonable speculation is that the connection compliance showed much less or even no influence on these two curves than the data in group 1. The extension-tension curve of one of these filaments is shown in Fig. 9.

In sum, for the majority of measurements, the connection resulted in a nonnegligible contribution to the measured elongation. After the exclusion of this contribution, the extension stiffness of a 1-μm-long actin filament was ~35 pN/nm, and the shape of length-tension curve remained almost the same.

Fit to the theory: the worm-like chain model

As a semiflexible polymer, the actin filament exhibits undulations because of its interactions with the surrounding solution (Kas et al., 1996). Based on the magnitude of such undulations, it has been possible to evaluate the persistence length, L_p, of free F-actin, which is in turn used to describe the filament's flexural rigidity (Yanagida et al., 1984; Gittes et al., 1993; Ott et al., 1993; Kas et al., 1984, 1996). When subjected to axial tension, the filament approaches its contour length, L_c, and such undulations should be progressively straightened out. The relationship between the filament-length change and exerted tension can be characterized either by a freely jointed chain model or a worm-like chain (WLC) model (Bustamante et al., 1994; Odjik, 1995; Marko and Siggia, 1995; Wang et al., 1997). The freely jointed chain model could not fit our data. In this section we fit our experimental data to a WLC model, which has been applied successfully to characterize the mechanical behavior of biopolymers such as DNA (Bustamante et al., 1994; Marko and Siggia, 1995; Wang et al., 1997) and titin (Kellermayer et al., 1997).

Several different WLC models have been derived for different applications (Bustamante et al., 1994; Odjik 1995; Marko and Siggia, 1995; Wang et al., 1997). One is the entropy WLC model, used to characterize the relationship between tension F and filament length L when the filament is stretched to lengths far below its contour length L_c (Bustamante et al., 1994):

$$\frac{FL_p}{k_bT} = \frac{1}{4}\left(1 - \frac{L}{L_c}\right)^{-2} - \frac{1}{4} + \frac{L}{L_c}, \qquad (4)$$

where k_b is Boltzmann constant, T is the absolute temperature in degrees Kelvin, and L_c is the filament-contour length.

This equation assumes that the polymer chain is inextensible, implying that all energy is used to stretch the polymer from a coiled/curved state to approach its contour length L_c. The polymer chains' entropic energy decreases accordingly. However, when the stretch is beyond contour length, this

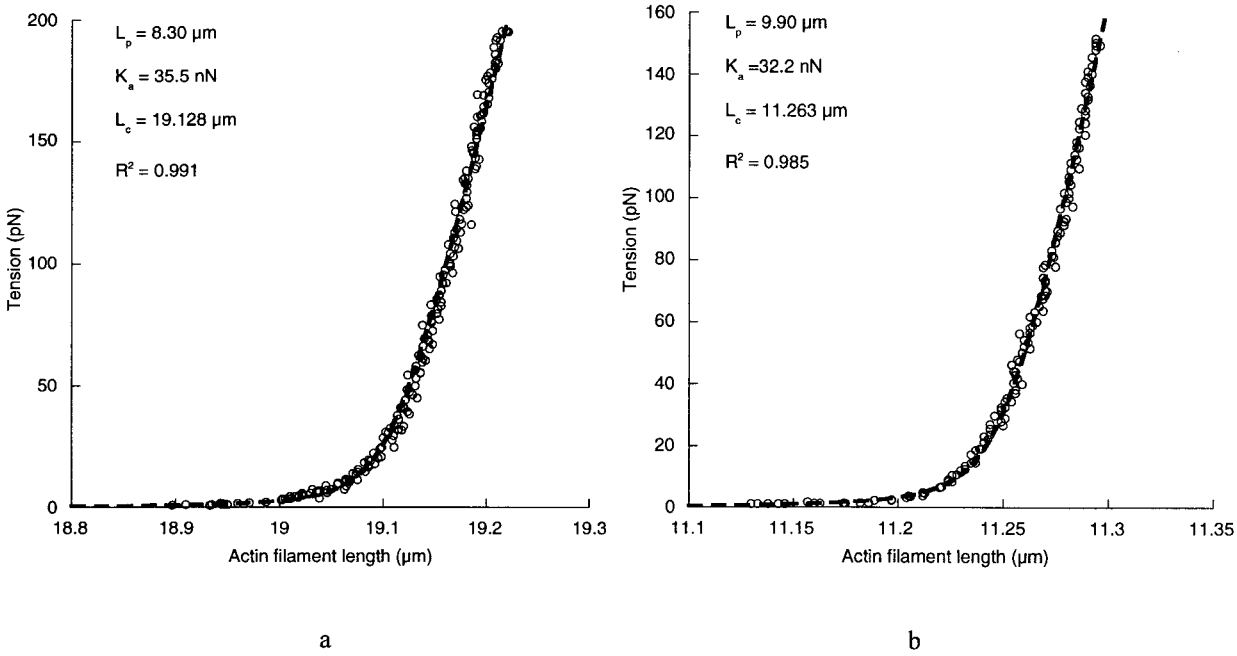

FIGURE 10 Fitting the data from actin filaments of length 19 μm (*a*) and 11.2 μm (*b*) with the entropy-enthalpy WLC model. The parameters shown here are the fit results. The dashed lines represent the fitted curve. See text for details.

equation is no longer valid. Thus, Wang et al. (1997) suggested the incorporation of an enthalpic elasticity term:

$$\frac{FL_p}{k_bT} = \frac{1}{4(1 - L/L_c + F/K_a)^2} - \frac{1}{4} + \frac{L}{L_c} - \frac{F}{K_a}, \qquad (5)$$

where K_a is the elastic stretch modulus of the long polymer chain unit.

These two models have been mainly used to characterize the mechanics of DNA and titin, whose tension-extension curves are dominated by the entropic term. However, for F-actin, neither of these two models could be used to fit our data. Odjik (1995) proposed that in the case of small elongation, i.e., $|L - L_c| \ll L$ and weak undulations, the following WLC model is applicable:

$$\frac{L}{L_c} = 1 - \frac{1}{2}\left(\frac{k_bT}{FL_p}\right)^{1/2} + \frac{F}{K_a} \qquad (6)$$

The first two terms in Eq. 6 are the asymptotic form of Eq. 4, describing the entropic stretching of the polymer chain as $L \to L_c$, so that they are the limit of Eq. 4. The third term assumes a linear change of polymer length with tension, which is depicted by the elastic stretch modulus K_a.

When using these models, one requirement must be borne in mind: filament length must be larger than persistence length. According to the reported persistence length of ~5–15 μm (Fujime et al., 1987; Takebayashi et al., 1977; Yanagida et al., 1984; Ott et al., 1993; Gittes et al., 1993), only several filaments in our experiments could meet that requirement. Using the curve shown in Fig. 10 *a*, in which the filament is as long as 19 μm, we found that neither the entropy model (Eq. 4) nor the modified entropy-enthalpy WLC model (Eq. 5) could fit our data well, whereas Eq. 6 is provisionally suitable for the entire tension range (1.5 pN). The best-fit parameters, $L_{p1} = 8.3$ μm, $K_{a1} = 35.5$ nN, and $L_{c1} = 19.1$ μm, are also illustrated in this figure, where the dashed line is the corresponding fitting curve.

The fitted persistence length of 8.3 μm falls within the range of ~5–15 μm as reported. When we attempted to apply this WLC model to filaments shorter than 10 μm, the persistence length was usually less than ~5 μm. For filaments longer than 10 μm the average persistence length was ~8.75 μm ($n = 9$) provided the data below 1.0 pN were excluded from the fit. Fig. 10 *b* demonstrates the results of another filament, ~11 μm long, the second filament of group 3 shown in Fig. 7. The persistence length is 9.9 μm.

The average tension at contour length was ~50 pN, which is equivalent to ~20% of the maximal physiological tension, P_0. This tension can also be computed by the expression $f^* = (k_bTK_a^2/4L_p)^{1/3}$. Given $K_a = 34.5$ pN/nm and $L_p = 8.75$ μm, the obtained tension is ~52 pN. It implies that the fitted persistence length is consistent with the elastic stiffness. If we take the length at the tension of 2.0 pN as the filaments' real initial length (different from the one measured before the filament was stretched), then the strains at contour length and at the peak of the linear portion (between the contour length and P_0) are both 0.4–0.6%.

As for the filaments in group 2, the fitted persistence length was usually ~1 μm and independent of filament

length. The fit parameters for an ~3.3-μm-long filament are shown in Fig. 6. The computed persistence length for these data was probably a reflection of the connection elasticity and therefore without physiological significance.

DISCUSSION

So far as we know, this is the first measurement of the complete actin-filament length-tension curve from zero tension to maximal physiological tension. At low tension the filament is highly compliant, and beyond a critical tension the curve bends sharply upward, continuing at almost constant slope, corresponding to a stiffness of ~34.5 ± 3.5 pN/nm. We propose that this behavior can be characterized by an entropy-enthalpy WLC model. Fitting the experimental data to this model gave a persistence length of ~8.75 μm. At extensions near contour length, the average tension was calculated to be ~50 pN, or ~20% of the physiological maximum.

Comparison with previous experiments

Filament elongation behavior could be divided into two portions: a nonlinear portion at low tension and a linear portion at moderate and high tensions. The nonlinearity at low tension was reported in previous investigations (Higuchi et al., 1995; Dupuis et al., 1997; Adami et al., 1999). For example, Adami and colleagues (1999) reported a nonlinear length-tension curve at tensions from 0 up to ~22 pN. Dupuis et al. (1997) measured single actin filament compliance using dual optical traps. However, the imposed maximal tension was as small as 7 pN. Both groups developed models to account for this nonlinearity. In the experiments of Higuchi et al. (1995) on thin filament compliance in skinned fibers, an exponential function was used to describe this nonlinearity. The thin filament was concluded to change compliance with the imposed tension. However, their data also showed that the compliance changed little with some additional increase of tension, implying that at high tension the compliance is tension independent.

Within the framework of the WLC model, these nonlinear relationships at low tensions reflect an entropic elasticity; i.e., the tension increase is mainly caused by overcoming entropy.

At moderate to high tensions, Kojima et al. (1994) concluded that in the range of ~35–190 pN the stiffness did not change with an increase of tension. This conclusion is in good agreement with our result, which reveals that only when the tension was higher than ~50 pN could the filament be elongated linearly. It also implies that when measuring the elastic stiffness of actin filaments (or any polymers that share similar characteristics) it is essential that the exerted force be high enough to stretch the polymer beyond its contour length. Kojima's measurements included only the high-tension region, and not the lower, nonlinear range.

The stiffness of 1-μm-long rhodamine-phalloidin-labeled F-actin reported by Kojima et al. (1994) was ~43 pN/nm, which agrees with our result, 34.5 ± 3.5 pN/nm, especially when the value at the release portion, i.e., ~40–44 pN/nm, was also taken into account. In their experiments, filaments were stretched to a predetermined tension and then oscillated with 20-Hz sinusoidal displacements. In our experiments, the stretch-release rate was much slower. The coincidence of stiffness values measured by the two different methods at different temporal scales reveals that the elasticity behavior is frequency independent, or nonviscoelastic, at least at the rates under investigation.

In addition to the direct stiffness measurements mentioned above, x-ray diffraction experiments on whole muscles (Huxley et al., 1994; Wakabayashi et al., 1994; Takezawa et al., 1998; Bordas et al., 1999) have also indicated substantial thin filament extensibility (~0.2–0.42%).

To compare our data quantitatively with x-ray results, it is necessary to estimate the amount of filament elongation that occurs when muscles contract isometrically from the resting state to P_0. This can be calculated from measured stiffness. However, in this study, we investigated pure F-actin whereas in muscle, actin filaments also contain other proteins such as troponin, tropomyosin (see Pollack, 1990), and nebulin. Both the direct stiffness measurements of Kojima et al. (1994) and the experiments of Goldmann (2000) on the bending stiffness of actin filaments revealed an ~50% stiffness increase with the addition of tropomyosin. If these proteins had been included, the measured stiffness might have been ~50–60% higher than pure F-actin, namely, ~51–55 pN/nm for stretch and ~60–70 pN/nm for release (for simplicity we take an average of stretch and release stiffness, i.e., ~60 pN/nm in the following estimations). From this adjusted value and given that the maximal physiological tension P_0 was assumed to be 230 pN as well as the tension at contour length to be 50 pN, the elongation of a 1-μm-long actin filament in the linear portion can be expressed as: (230 − 50) pN/60 pN/nm = 3 nm. This corresponds to a strain of 0.3%, revealing that our result is in good agreement with x-ray diffraction data.

In quick release experiments (Huxley and Simmons, 1971; Ford et al., 1977) the length change has been interpreted as a reflection of cross-bridge elasticity. Our results imply that that much of the elasticity apparently resides in the thin filaments. Indeed, recent stiffness measurements made on isolated vertebrate thick filaments have also shown substantial compliance, with strain on the order of ~1.5% over the physiological range (Dunaway et al., 2002). Hence, much of the sarcomere compliance may well reside in filaments.

TABLE 1 Dependence of persistence length on the start points

Start point					
Filament slack length (μm)	Tension (nN)	Persistence length (μm)	Stretch modulus (nN)	Contour length (μm)	R^2
18.89	>0.1	17.8	30.2	19.11	0.98
18.94	>1.0	8.3	35.7	19.13	0.99
19.00	>2.0	6.74	38.89	19.137	0.99
19.01	>3.0	6.17	39.91	19.139	0.99
19.02	>4.0	6.0	40.2	19.14	0.99

Persistence length

Various methods have been used to estimate the persistence length of F-actin filament. Studies using light-scattering and electron microscopy (Fujime et al., 1987; Takebayashi et al., 1977) gave values of 6 μm. Observations of thermally driven fluctuations of F-actin gave estimates of ~10–17.5 μm (Yanagida et al., 1984; Ott et al., 1993; Gittes et al., 1993).

To our knowledge, this is the first time that the WLC model has been used to quantitatively describe the nonlinear behavior of F-actin in the low-tension range. From the fit, an estimation of the persistence length of ~8.75 μm was obtained, which fell in the range of reported values, ~5–17 μm.

However, using a method similar to ours, Kas et al. (1996) reported a persistence length of 1.8 μm for short-wavelength thermal undulation modes, whereas their value could become as high as 10 ± 5 μm in the long-wavelength regime. During data analysis we found similar behavior. For example, the persistence length of 8.3 μm shown in Fig. 10 *a* could be as high as ~17.8 μm when the data lower than 1 pN were incorporated in the fit. The more the data were cut off in the low-tension range, the smaller the computed persistence length and the bigger the stretch modulus, as illustrated in Table 1.

One possibility, as proposed by Kas et al. (1996), to account for this phenomenon is that for undulations in the long-wavelength regime, other modes besides bending are excited, which are no longer suitable for bending modulus calculations. In our case, before being stretched filaments were in a slack state. Intuitively, the slacker the filament (and thus the shorter the filament's length) the more easily the long-wavelength undulation could be elicited and the more easily the undulations could be disturbed by the limit size of the chamber or the boundary conditions imposed by the two levers. As demonstrated in Table 1, apparently, the slacker the filament (the shorter the contour length), the larger the fitted persistence length. The given persistence length of ~8.75 μm was obtained with the exclusion of data lower than 1 pN.

Alternatively, when the tension is below 1 pN, the undulations magnitude may be too large to meet the weak undulation requirement of Eq. 6.

In sum, the nano-lever manipulation method has provided the means by which the elastic behavior of single F-actin could be studied from zero tension to maximum physiological tension, thereby providing full characterization of F-actin elasticity. We found nonlinear behavior at low tension and linear behavior at higher tension, which represents a constant stiffness of 34.5 ± 3.5 pN/nm for stretch and ~40–44 pN/nm for release. By fitting data with an entropy-enthalpy WLC model, we obtained a persistence length of ~8.75 μm. The measured stiffness implies that filaments can be stretched by ~0.3% when tension is increased from contour length to P_0, which is consistent with x-ray diffraction results.

REFERENCES

Adami, R., D. Choquet, and E. Grazi. 1999. Rhodamine phalloidin F-actin: critical concentration versus tensile strength. *Eur. J. Biochem.* 263: 270–275.

Bordas, J., A. Svensson, M. Rothery, J. Lowy, G. P. Diakun, and P. Boesecke. 1999. Extensibility and symmetry of actin filaments in contracting muscles. *Biophys. J.* 77:3197–3207.

Bustamante, C., J. F. Marko, E. D. Siggia, and S. Smith. 1994. Entropic elasticity of lambda-phage DNA. *Science.* 265:1599–1600.

Dunaway, D., M. Fauver, and G. H. Pollack. 2002. Direct measurement of single vertebrate thick filament elasticity using nanofabricated cantilevers. *Biophys. J.* 82:3128–3133.

Dupuis, D. E., W. H. Guilford, J. Wu, and D. M. Warshaw. 1997. Actin filament mechanics in the laser trap. *J. Muscle Res. Cell Motil.* 18: 17–30.

Fauver, M. E., D. L. Dunaway, H. L. Lilienfeld, H. G. Craighead, and G. H. Pollack. 1998. Microfabricated cantilevers for measurement of subcellular and molecular forces. *IEEE Trans. Biomed. Eng.* 45:891–898.

Ford, L. E., A. F. Huxley, and R. M. Simmons. 1977. Tension responses to sudden length change in stimulated frog muscle fibres near slack length. *J. Physiol.* 269:441–515.

Ford, L. E., A. F. Huxley, and R. M. Simmons. 1981. The relation between stiffness and filament overlap in stimulated frog muscle fibres. *J. Physiol.* 311:219–249.

Fujime, S., O. M. Takasaki, and S. Ishiwata. 1987. Dynamic light-scattering study of muscle F-actin. II. *Biophys. Chem.* 27:211–224.

Gittes, F., B. Mickey, J. Nettleton, and J. Howard. 1993. Flexural rigidity of microtubules and actin filaments measured from thermal fluctuations in shape. *J. Cell Biol.* 120:923–934.

Goldmann, W. H. 2000. Binding of tropomyosin-troponin to actin increases filament bending stiffness. *Biochem. Biophys. Res. Commun.* 276:1225–1228.

Higuchi, H., T. Yanagida, and Y. E. Goldman. 1995. Compliance of thin filaments in skinned fibers of rabbit skeletal muscle. *Biophys. J.* 69: 1000–1010.

Huxley, A. F., and R. M. Simmons. 1971. Proposed mechanism of force generation in striated muscle. *Nature.* 233:5333–5338.

Huxley, H. E., A. Stewart, H. Sosa, and T. Irving. 1994. X-ray diffraction measurements of the extensibility of actin and myosin filaments in contracting muscle. *Biophys. J.* 67:2411–2421.

Kas, J., H. Strey, and E. Sackmann. 1984. Direct imaging of reptation for semiflexible actin filaments. *Nature.* 368:226–229.

Kas, J., H. Strey, J. X. Tang, D. Finger, R. Ezzell, E. Sackmann, and P. A. Janmey. 1996. F-actin, a model polymer for semiflexible chains in

dilute, semidilute, and liquid crystalline solutions. *Biophys. J.* 70: 609–625.

Kellermayer, M. S., S. B. Smith, H. L. Granzier, and C. Bustamante. 1997. Folding-unfolding transitions in single titin molecules characterized with laser tweezers. *Science.* 276:1112–1116.

Kojima, H., A. Ishijima, and T. Yanagida. 1994. Direct measurement of stiffness of single actin filaments with and without tropomyosin by in vitro nanomanipulation. *Proc. Natl. Acad. Sci. U.S.A.* 91:12962–12966.

Marko, J. E., and E. D. Siggia. 1995. Stretching DNA. *Macromolecules.* 28:8759–8770.

Neumann, T., M. Fauver, and G. H. Pollack. 1998. Elastic properties of isolated thick filaments measured by nanofabricated cantilevers. *Biophys. J.* 75:938–947.

Odjik, T. 1995. Stiff chains and filaments under tension. *Macromolecules.* 28:7016–7018.

Oosawa, F. 1977. Actin-actin bond strength and the conformational change of F-actin. *Biorheology.* 14:11–19.

Oosawa, F. 1980. The flexibility of F-actin. *Biophys. Chem.* 11:443–446.

Oosawa, F., Y. Maeda, S. Fujime, S. Ishiwata, T. Yanagida, and M. Taniguchi. 1977. Dynamic characteristics of F-actin and thin filaments in vivo and in vitro. *J Mechanochem. Cell Motil.* 4:63–78.

Ott, A., M. Magnasco, A. Simon, and A. Libchaber. 1993. Measurement of the persistence length of polymerized actin using fluorescence microscopy. *Phys. Rev. E.* 48:R1642–R1645.

Pardee, J. D., and J. A. Spudich. 1982. Purification of muscle actin. *Methods Enzymol.* 85:164–181.

Pollack, G. H. 1990. Muscles and Molecules: Uncovering the Principles of Biological Motion. Ebner and Sons Publishers, Seattle.

Schutt, C. E., and U. Lindberg. 1992. Actin as the generator of tension during muscle contraction. *Proc. Natl. Acad. Sci. U.S.A.* 89:319–323

Takebayashi, T., Y. Morita, and F. Oosawa. 1977. Electronmicroscopic investigation of the flexibility of F-actin. *Biochim. Biophys. Acta.* 492: 357–363.

Takezawa, Y., Y. Sugimoto, and K. Wakabayashi. 1998. Extensibility of the actin and myosin filaments in various states of skeletal muscle as studied by x-ray diffraction. *Adv. Exp. Med. Biol.* 453:309–317.

Wakabayashi, K., Y. Sugimoto, H. Tanaka, Y. Ueno, Y. Takezawa, and Y. Amemiya. 1994. X-ray diffraction evidence for the extensibility of actin and myosin filaments during muscle contraction. *Biophys. J.* 67: 2422–2435.

Wang, M. D., H. Yin, R. Landick, J. Gelles, and S. M. Block. 1997. Stretching DNA with optical tweezers. *Biophys. J.* 72:1335–1346.

Yanagida, T., M. Nakase, K. Nishiyama, and F. Oosawa. 1984. Direct observation of motion of single F-actin filaments in the presence of myosin. *Nature.* 307:58–60.